J Mater Sci (2019) 54:6709–6718

Polymers

Nanocellulose-based magnetic hybrid aerogel for adsorption of heavy metal ions from water

Jie Wei[1], Zhixing Yang[1], Yun Sun[1], Changkai Wang[1], Jilong Fan[1], Guoyin Kang[1], Rong Zhang[1], Xiaoying Dong[1,*], and Yongfeng Li[1,*]

[1] *Department of Wood Science and Engineering, Forestry College, Shandong Agricultural University, No. 61 Daizong Road, Taian 271018, China*

Received: 30 November 2018
Accepted: 2 January 2019
Published online: 8 January 2019

ABSTRACT

Heavy metal pollution is one of the most serious environmental problems, posing threats to human health. Here, we developed a magnetic hybrid aerogel by integrating nanocellulose and ferroferric oxide (Fe_3O_4) nanoparticles for effectively adsorbing heavy metal ions from water and realizing controllable recovery under magnetic condition. The magnetic behavior and adsorbing capacity of the hybrid aerogel on removal of heavy metal chromium (Cr)(VI) ion were examined. Results show that the ferroferric oxide nanoparticles physically adsorb the nanocellulose, each of which retains the original composition and structural characteristics. The magnetic hybrid aerogel possesses good ferromagnetic property with saturation magnetization value of 53.69 emu/g, enabling effective and controllable recovery of the aerogel under magnetic condition The adsorption efficiency of the hybrid aerogel on the Cr(VI) ion reaches the highest value of 2.2 mg/g when the mass ratio of the nanocellulose to ferroferric oxide nanoparticle is 1:1. Additionally, the hybrid aerogel presents similar adsorption behavior on plumbum (Pb)(II) and copper (Cu)(II) ions, suggesting extended applications of the hybrid aerogel on removal of heavy metal ions. Such strategy could provide new applications for the abundant nanocellulose resources and could be extended to integrate nanocellulose with other functional nanomaterials into novel hybrid aerogel for water purification.

Jie Wei, Zhixing Yang, Yun Sun, Changkai Wang and Jilong Fan have contributed equally to this work.

Address correspondence to E-mail: dxiaoying1982@163.com; yfli@sdau.edu.cn; lyf288@hotmail.com

https://doi.org/10.1007/s10853-019-03322-0

Introduction

Water pollution poses a great threat to human survival, which has driven greatest attentions from all the countries [1, 2]. It is normally originated from the chemical industries, agricultural pollution source, oil spill and household wastes, which mainly consist of organic chemicals (like dyes and detergents), oil, fertilizer and pesticide, inorganic chemicals and heavy metal ions [3–6]. Among them, the heavy metal pollution is recognized as the most serious harm due to its undegradability and enrichment in water [7]. The heavy metal ions typically include hydrargyrum (Hg)(II), chromium (Cr)(VI), plumbum (Pb)(II), copper (Cu)(II), stannum (Sn)(II) and so on. Many researches have been reported to address the big problem of water pollution caused by heavy metal ions, including chemical precipitation, physical adsorption, ion exchange and biological treatment [8–10]. Therein, the adsorption way is the most popular one due to its easy process and environmental friendliness, which realizes its function via the strong adsorption behavior of porous materials with tremendous pores in micro-/nanoscale [11–14]. Consequently, active carbon, especially aerogels as key objects, is typically explored to remove heavy metal ions via their huge adsorption capacity [15–17]. However, the most explored aerogels are derived from materials, like nanosilica, graphene oxide, polydimethylsiloxane foam and active carbon, which are non-renewable, non-degradable and costly [18–20]. Therefore, developing green and environment-friendly aerogels from renewable materials instead of non-renewable materials to overcome the above big challenges is desirable and interesting.

Cellulose is the most widely distributed biopolymer in nature, whose annual output on earth is up to 75 billion tons [21, 22]. It is mainly originated from biomass plants like trees, straws and vines [23]. Nanocellulose with mean diameter in nanoscale and length in microscale can be isolated from the above natural biomass materials by mechanical, chemical and/or biological methods [24–28]. The nanoscale biopolymer possesses large specific surface area, high aspect ratio, excellent mechanical properties and abundant hydroxyl groups, positioning an ideal building block for aerogels with density lower than air, compression ratio higher than 99% and various functionalities [29–31]. Zhu et al. [32] designed a nanocellulose-based hybrid aerogel with nanocellulose as framework that effectively removed heavy metal ion [Cr(VI)] and benzotriazole from water. Geng et al. [33] developed a 3-mercaptopropyltrimethoxysilane-modified nanocellulose aerogel which effectively removed Hg(II) from water with efficiency of 85 mg L^{-1}. Yao et al. [34] prepared a nanocellulose aerogel decorated with aldehyde group, which being applied as mesoporous sorbent to remove Pb(II) and Cu(II) from aqueous solution, along with capacity of 0.75 mmol g^{-1} and 0.58 mmol g^{-1}, respectively. Despite their effective removal of the heavy metal ions from water, they could not realize recovery under controlled conditions which is necessary and important for practical applications. In particular, the studies on the controllable recovery of nanocellulose-based aerogel are rarely reported [35–37]. Thus, developing recyclable nanocellulose-based aerogel under controlled condition toward water purification is interesting but challenging.

In this context, we build a nanocellulose-based hybrid aerogel to remove heavy metal ions from water under magnetic condition. Nanocellulose extracted from shrub plant and nano-Fe_3O_4 particles are employed to design the recyclable aerogel for demonstration. The resulted hybrid aerogel realizes maximum removal of Cr(VI) ion with adsorption rate of 2.2 mg/g and effective recovery under magnetic condition, suggesting effective adsorption behavior and controllable recyclability of the designed aerogel. In addition, the hybrid aerogel also presents adsorption features on removal of Pb(II) and Cu(II) ions. Such strategy could provide new applications for the abundant nanocellulose resources.

Materials and methods

Materials

Amorpha fruticosa was obtained from the suburb of Tai'an city in China, and the limb was crushed into 100-mesh powder by a plant crusher. Nano-Fe_3O_4 with diameter of ~ 20 nm was purchased from Shanghai McLean Co., Ltd (Shanghai, China). Benzene, anhydrous ethanol, glacial acetic acid, sodium acetate, ammonia, potassium oxide, potassium chromate, phosphoric acid, sulfuric acid and anhydrous copper sulfate were purchased from Tianjin Kay

Tong Chemical Reagent Co., Ltd. (Tianjin, China). Sodium chlorite, diphenylcarbazide, xylenol orange, sodium diethyldithiocarbamate and lead nitrate were obtained from Shandong West Asia Chemical Industry Co., Ltd. (Linyi, China).

Methods

Preparation of nanocellulose

The dried *A. fruticosa* wood powder (2.5 g, 100-mesh screening) was extracted using Soxhlet extractor along with benzene–ethanol solution at a volume ratio of 2:1 for 6 h. The lignin was then removed using sodium chlorite under acidic condition (pH 4 to 5, adjusted by glacial acetic acid) for 6 h (1 h each cycle, repeated 6 cycles). And the hemicellulose was subsequently removed by twice treatments of potassium hydroxide (2 h for each treatment). Finally, the water suspension of the purified cellulose with a mass concentration of 0.3 wt% was treated to obtain nanocellulose suspension via processes of 600-bar treatment of high-pressure homogenization for 20 min, followed by 800 W ultrasonic treatment for 20 min, which could be stably suspended for more than 1 month.

Preparation of nanocellulose-Fe_3O_4 hybrid aerogel

First, *A. fruticosa* Linn. as a typical shrub plant is employed to extract nanocellulose (Fig. 1a), which is further designed to integrate nano-Fe_3O_4 particles into the mixed solution. Then, the mixture was stirred at 300 rpm for 10 min, followed by an ultrasonic treatment under 500 Hz for 2 h. Finally, the mixture was freeze-dried under conditions of − 55 °C and 1 Pa to obtain the nanocellulose-Fe_3O_4 hybrid aerogel (Fig. 1b). It contains a hierarchical porous structure with a great many pores in micro-/nanoscale, which theoretically features huge adsorption capacity. Such structural design for the aerogel is expected to remove heavy metal ions from waste water and to realize controllable recovery under magnetic condition (Fig. 1c). The hybrid aerogels with 15 kinds of mass ratio were explored. The employed mass ratios of nanocellulose and nano-Fe_3O_4 particles include 0:1, 1:4, 1:3, 1:2, 1:1, 2:1, 3:1, 4:1, 5:1, 6:1, 7:1, 8:1, 9:1, 10:1, 1:0.

Microscopic characterization

The microstructures of nanocellulose and the nanocellulose-Fe_3O_4 hybrid aerogel were observed by scanning electron microscopy (FE-SEM, JSM-6610LV, JEOL USA Inc., Peabody, Massachusetts) and transmission electron microscope (TEM, JEM-1400, JEOL USA Inc., Peabody, Massachusetts). For the SEM observation, the test conditions were high vacuum mode, working voltage of 12.5 kV and beam spot of 5.0. For the TEM observation, the nanocellulose suspension was dropped onto copper screen, then

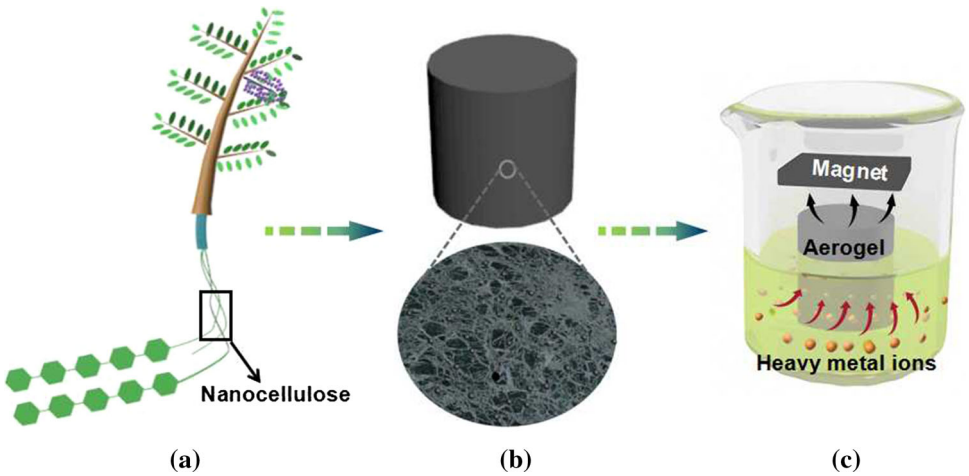

Figure 1 Schematic illustration of the hybrid aerogel derived from the shrub plant and its adsorption behavior on removal of heavy metal ions from sewage under controlled condition. **a** Nanocellulose obtained from the shrub plant, *Amorpha fruticosa* Linn., **b** nanocellulose–ferroferric oxide hybrid aerogel and **c** adsorption behavior of the hybrid aerogel on removal of the heavy metal ions and its controlled recovery under magnetic condition.

negatively stained by phosphotungstic acid and finally dried at room temperature before examination.

Characterization of chemical composition

XPS tests on nanocellulose, ferroferric oxide nanoparticles and nanocellulose-Fe_3O_4 hybrid aerogels were performed using a K-alpha system (ESCALAB 250Xi, Thermo Scientific Inc., Waltham, Massachusetts) operated at 14.0 kV. The FTIR spectra were obtained using a Nicolet Magna 560 FTIR instrument (Thermo Nicolet Inc., Wisconsin, Madison). The test parameters were resolution of 4 cm^{-1} and number of scans 32. The sample was placed on the stage of the diamond ATR accessory, and the pressure column was adjusted to the appropriate location for the test. The Raman scattering measurement was taken using a Raman system (LabRAM HR Evolution, HORIBA Jobin Yvon Inc., Paris, France) at room temperature. The solid-state diode laser (532 nm and 633 nm) was used as an excitation source with a frequency range of 4000–500 cm^{-1}. The crystal structure and crystallinity of the samples were analyzed by X-ray diffractometer (XRD, D/max 2200, Rigaku Americas Corporation, Woodlands, Texas). The test parameters include a copper target, ray wavelength of 0.154 nm, scanning angle from 5° to 60°, scanning speed of 4°/min, step of 0.02°, voltage of 40 kV and current of 30 mA. The concentration of heavy metal ions [Cr(VI), Pb(II), Cu(II)] was measured by an UV–Vis spectrometer (Cary 50, Xiamen Yichen Technology Inc., China).

Test of vibration sample magnetization

Vibrating sample magnetometer (VSM) (superconducting quantum interference device (SQUID)-VSM, Quantum Design, Inc., San Diego, California) was used to test the magnetization intensity of the nanocellulose-Fe_3O_4 hybrid aerogel. The test parameters included temperature of 300 K and the magnetic field range of − 20000–20000 Oe. The sample size was $1 \times 1 \times 1$ mm^3.

Measurement of density and porosity

The density of nanocellulose-Fe_3O_4 hybrid aerogel was calculated using the following equation:

$$\rho = \frac{m}{v} \tag{1}$$

where ρ is the density of the nanocellulose-Fe_3O_4 hybrid aerogel, m is the weight of nanocellulose-Fe_3O_4 hybrid aerogel and v is the volume of nanocellulose-Fe_3O_4 hybrid aerogel.

The porosity of nanocellulose-Fe_3O_4 hybrid aerogel is calculated using the following formula [38]:

$$P(\%) = 100 \times \left\{1 - \left[\left(\rho \times {}^{n}/_{(n+1)}\right)/\rho_a\right] - \left(\rho \times {}^{1}/_{(n+1)}\right)/\rho_b\right\} \tag{2}$$

where P is the porosity of nanocellulose-Fe_3O_4 hybrid aerogel, ρ is the density of nanocellulose-Fe_3O_4 hybrid aerogel, ρ_a and ρ_b are the density of nanocellulose (1.59 g/cm^3) and nano-Fe_3O_4 particles ($\sim$ 5.18 g/cm^3), respectively, and n is the fraction of nanocellulose in nanocellulose-Fe_3O_4 hybrid aerogel.

Heavy metal adsorption

First, the three heavy metal ions, i.e., Cr(VI), Pb(II) and Cu(II) ion, were, respectively, prepared into standard solution according to the reported methods: diphenylcarbazide spectrophotometric determination for Cr(VI) ion [9], xylenol orange spectrophotometric determination for Pb(II) ion [39] and sodium diethyldithiocarbamate spectrophotometric determination for Cu(II) ion [40]. Secondly, each standard solution with six volumes at 1 mL, 2 mL, 4 mL, 6 mL, 8 mL and 10 mL was, respectively, poured into a 50-mL colorimetric tube to measure the absorbances (Abs) of the heavy metal ions via a UV–Vis spectrophotometer. The UV–Vis absorption spectroscopy at the maximum absorption wavelength of 540 nm, 575 nm and 450 nm was, respectively, used to estimate the adsorption behavior of the hybrid aerogel toward Cr(VI), Pb(II) and Cu(II) ion. Thirdly, the standard curve for each heavy metal ion was accordingly drawn in terms of the above three methods (Fig. 2).

In the equilibrium adsorption experiment, the nanocellulose-Fe_3O_4 hybrid aerogel was first put in 50 mL solution containing heavy metal ion at concentration of 3 mg/L. Then, the solution was shaken by an orbital shaker at 120 r/min for several hours; after that, the hybrid aerogel was removed from the solution by a magnet. The absorbance of the solution

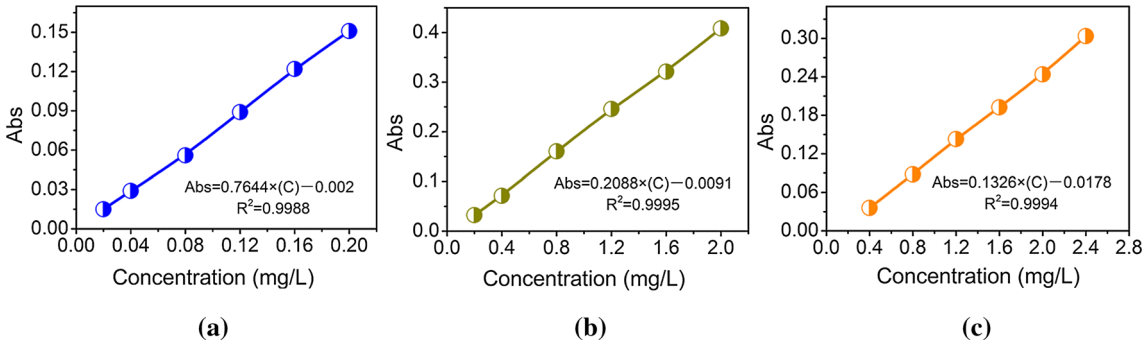

Figure 2 Standard curves of the heavy metal ions. **a** Standard curve for Cr(VI) ion, **b** standard curve for Pb(II) ion and **c** standard curve for Cu(II) ion.

was subsequently examined by a UV spectrophotometer. The content (mg/mL) of the remaining heavy metal ion in the solution after aerogel adsorption could be further calculated in terms of the above standard curves. And the adsorption capacity of the hybrid aerogel is finally calculated according to formulae 3 and 4:

$$C = \frac{m}{v} \tag{3}$$

C (mg/mL) represents the heavy metal ion concentration; m (mg) indicates the mass of the heavy metal ion in the solution; and v is the solution volume (mL).

$$R = \frac{(C_i - C_f)}{m_a} \times v \tag{4}$$

R (mg/g) indicates the adsorption amount of heavy metal ion at equilibrium; C_i (mg/mL) represents the initial concentration of the heavy metal ion in the solution; C_f is the final concentration of the heavy metal ion in the solution; m_a (g) indicates the mass of the aerogel; and v represents the volume.

Results and discussion

Figure 3a shows that the nanocellulose suspension is stable without obvious flocculation, indicating uniform dispersion of the nanocellulose in aqueous solution. Figure 3b presents the nanocellulose in fine structure with length over 10μm and diameter under 100 nm. Figure 3c proves that the diameter of the nanocellulose is mainly in the range of 20–100 nm with mean value of ~ 50 nm, indicating high aspect ratio of the nanocellulose greater than 200. Figure 3d exhibits the hybrid aerogel stood on plant leaf, suggesting extremely lower density. In fact, the mean density is ~ 5 mg/cm^3, slightly higher than that of air, which should be ascribed to the interesting porous structure (Fig. 3e, S1; Table 1). It contains huge amounts of pores with diameters in microscale and nanoscale, enabling a hierarchical porous structure for large adsorption capacity. The magnified SEM image shows that the nano-Fe_3O_4 particles evenly coated nanofibers to form the nanocellulose-Fe_3O_4 composite, though their interaction should be physical force due to the lack of chemical bonds between them (Fig. 3f, S2, S3). Such unique structure theoretically endows the hybrid aerogel with great adsorption capacity and magnetic response behavior [36].

Figure 4 further confirms the above analysis on the chemical components and their interactions. As shown in Fig. 4a, the nanocellulose presents obvious diffraction peak at $2\theta = 16.2°$ and $2\theta = 22.3°$, indicating type I crystalline structure of the nanocellulose without crystal change. Ferroferric oxide nanoparticle shows diffraction peaks at 18.3°, 30.1°, 35.4°, 43.1°, 53.4° and 56.9°, corresponding to lattice plane of (111), (220), (311), (400), (422) and (511), respectively. The XRD curve of the hybrid aerogel well matches those of nanocellulose and Fe_3O_4 without new diffraction peak appeared, indicating physical interaction between nanocellulose and Fe_3O_4 and thus proving the above analysis. The XPS curve of the hybrid aerogel enables the identifications of Fe element from Fe_3O_4 and C element from nanocellulose (Fig. 4b). The FTIR spectra present that the stretching vibrations of –OH group at 3200–3400 cm^{-1}, –CH group at 2900 cm^{-1} and C–O group at 1030 cm^{-1} assign to the nanocellulose, and obvious vibrating peak is absent in Fe_3O_4 spectra (Fig. 4c). The hybrid aerogel presents similar spectra to that of nanocellulose without new vibrating peaks, indicating physical

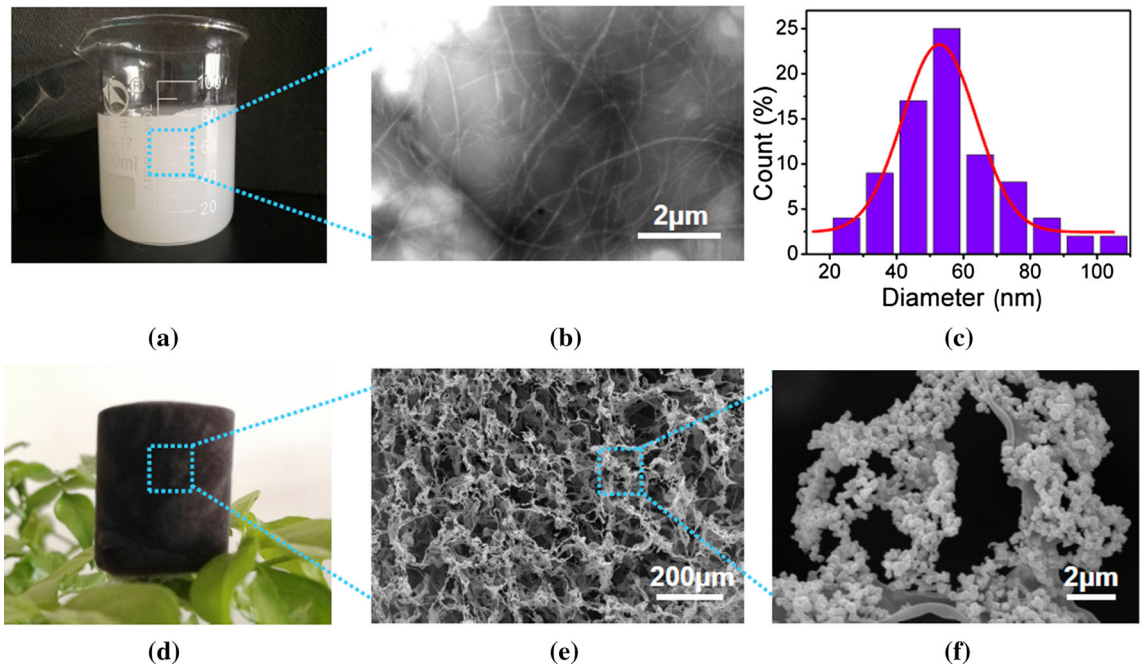

Figure 3 Morphologies of nanocellulose and the nanocellulose-Fe_3O_4 hybrid aerogel. **a** Digital photograph of the nanocellulose suspension, **b** TEM image of the nanocellulose, **c** diameter statistic of the nanocellulose from the TEM image, **d** digital photograph of the hybrid aerogel, **e** SEM image of the hybrid aerogel and **f** magnified SEM image of the hybrid aerogel.

Table 1 Relationship of density and porosity of the hybrid aerogel with the mass ratio of nanocellulose to nano-Fe_3O_4 particles

Mass ratio of nanocellulose to nano-Fe_3O_4	Density (mg/cm^3)	Porosity (%)
1:1	7.01	99.71
2:1	6.98	99.66
3:1	5.02	99.74
4:1	4.75	99.74
5:1	4.78	99.74
6:1	5.01	99.72
7:1	4.93	99.72
8:1	4.50	99.74
9:1	4.33	99.75
10:1	3.31	99.81

interaction between nanocellulose and Fe_3O_4 without chemical bonds. This is consistent with the analysis result of XRD characterization. The Raman spectra also present the characteristic peak of –CH group at 2895 cm^{-1}, assigning to nanocellulose (Fig. 4d). However, there are no new peaks different from the characteristic peaks of nanocellulose and Fe_3O_4 appeared in the Raman spectra of the hybrid aerogel, indicating the absence of chemical bonds between nanocellulose and Fe_3O_4 in the hybrid aerogel. Consequently, we conclude that the nanocellulose and nano-Fe_3O_4 particles combiningly form the hybrid aerogel via physical interaction.

Such hybrid aerogel presents magnetic property due to the existence of the nano-Fe_3O_4 particles [5, 41, 42]. Figure 5a shows that the magnetization of the hybrid aerogel increases with the external magnetic intensity and presents magnetic saturation of 53.69 emu/g. The magnetization direction coincides with the direction of the applied magnetic field, indicating obvious ferromagnetism of the hybrid aerogel. Such magnetic feature is beneficial to the effective recovery of the hybrid aerogel under magnetic condition.

After the hybrid aerogel being placed into the water solution containing Cr(VI) ion, the solution

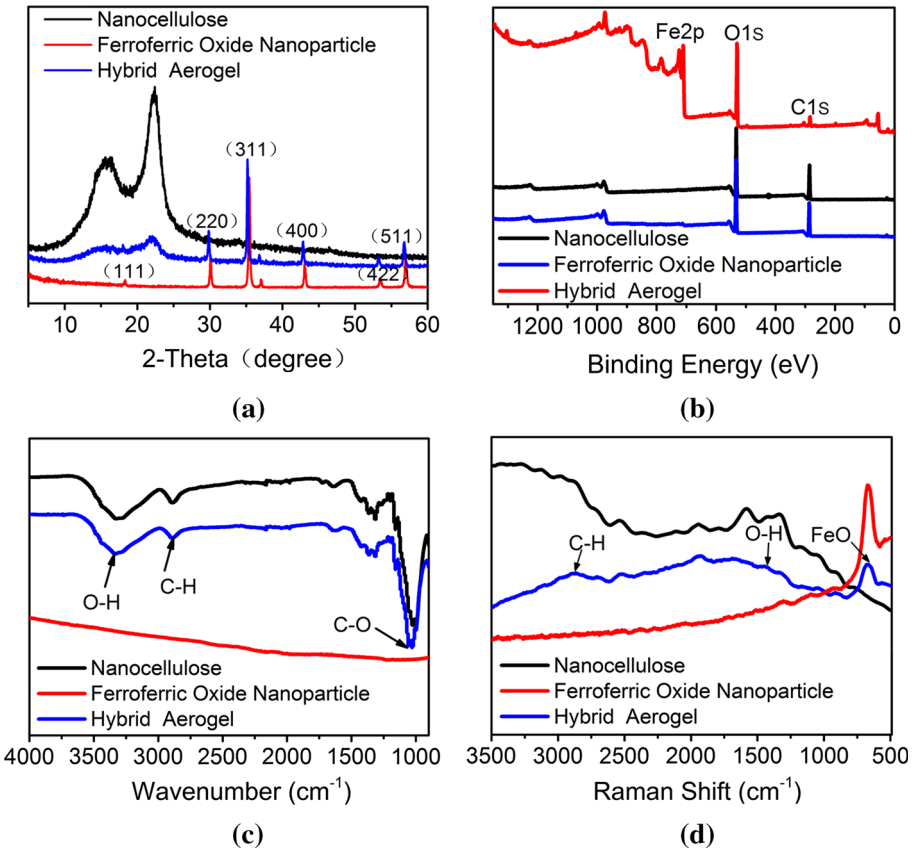

Figure 4 Characterizations of nanocellulose, ferroferric oxide nanoparticles and the nanocellulose-Fe_3O_4 hybrid aerogel. **a** XRD curves of nanocellulose, ferroferric oxide nanoparticles and the nanocellulose-Fe_3O_4 hybrid aerogel, **b** XPS spectra of nanocellulose, ferroferric oxide nanoparticles and the nanocellulose-Fe_3O_4 hybrid aerogel, **c** FTIR spectra of nanocellulose, ferroferric oxide nanoparticles and the nanocellulose-Fe_3O_4 hybrid aerogel and **d** Raman spectra of nanocellulose, ferroferric oxide nanoparticles and the nanocellulose-Fe_3O_4 hybrid aerogel.

color gradually changes from yellow to colorless (Fig. 5b). Figure 5b and Movie S4 also present that the hybrid aerogel could be lifted out of the solution by a magnet, indicating the magnetic characteristic of the hybrid aerogel. The concentration of the solution before and after adsorption is further qualitatively determined by a UV–Vis spectrometer, respectively. The absorption peak at 540 nm, corresponding to the maximum absorption of Cr(VI) ion, drops drastically from before to after adsorption, suggesting effective removal of the heavy metal ion from water via the aerogel adsorption behavior (Fig. 5c). The aerogel at different mass ratios presents different adsorption capacity on removal of Cr(VI) ion. When the mass ratio of the nanocellulose to nano-Fe_3O_4 is 1:1, the adsorption capacity of the hybrid aerogel reaches the maximum value of 2.2 mg/g (Fig. 5d), which is much better than that of the previously reported adsorbents (Fig. 5e) [43–48]. The fact should be ascribed to the high porosity of the aerogel over 99% due to the hierarchical micro-/nanoscale structure and the high specific surface area of nanocellulose and the nano-Fe_3O_4 particles (Table 1). Notably, the adsorption capacity of the hybrid aerogel at mass ratio of 1:1 increases with the porosity, proving the effectiveness of the porosity (Fig. S4). However, when the mass ratio is lower than 1:1, the aerogel could not stably suspend in the solution due to less nanocellulose. We therefore confirm that the optimal mass ratio of the nanocellulose to the nano-Fe_3O_4 is 1:1. In addition, the hybrid aerogel with mass ratio of 1:1 can also adsorb Pb(II) ion and Cu(II) ion from water, with maximum value of 1.25 mg/g and 0.4 mg/g, respectively, indicating such hybrid aerogel is capable of removing other kinds of metal ions from water (Fig. 5f, S5, S6). Such results suggest that the design could extend the nanocellulose to be tailored into functional aerogel, which could effectively purify water and realize controlled recovery under magnetic condition.

Conclusions

Upon the high aspect ratio of the nanocellulose to the magnetic feature of nano-Fe_3O_4, we successfully designed the nanocellulose-Fe_3O_4 hybrid aerogel to adsorb heavy metal ions for water purification and to

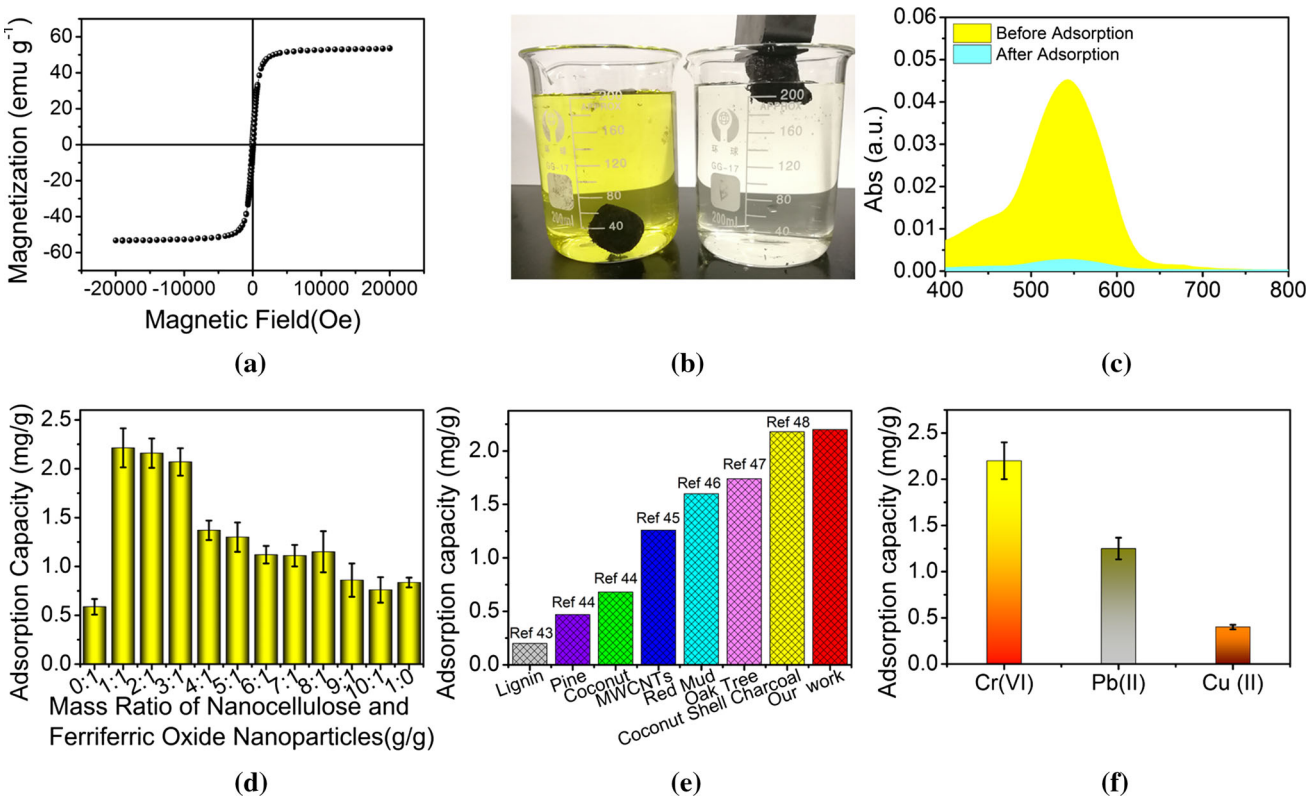

Figure 5 Magnetic property and adsorption efficiency of the nanocellulose-Fe_3O_4 hybrid aerogel. **a** Hysteresis curve of the hybrid aerogel, **b** digital photograph to show the solution color change before and after Cr(VI) ion removal by the hybrid aerogel, **c** UV–Vis absorbance spectra of the Cr(VI) ion solution before and after absorption, **d** adsorption capacity of the hybrid aerogel at different mass ratios for the Cr(VI) ion, **e** comparison of the maximum adsorption capacity of various adsorbents on removal of Cr(VI) ion and **f** comparison of the maximum adsorption capacity of the hybrid aerogel on removal of Cr(VI), Pb(II) and Cu(II) ions.

realize controllable recovery under magnetic condition. The hybrid aerogel presents ferromagnetic characteristic with saturation magnetization of 53.69 emu/g and reaches effective removal of Cr(VI) ion with the maximum removal capacity of 2.2 mg/g when the mass ratio of nanocellulose to nano-Fe_3O_4 is 1:1. The hybrid aerogel also demonstrates adsorption behavior on removal of Pb(II) and Cu(II) ions from water. Such design extends the nanocellulose to be potentially applied in water purification and makes it realize controllable recovery under magnetic condition.

Acknowledgements

We acknowledge the financial supports from the Natural Science Foundation of Shandong Province, Doctoral Branch (Grant No. ZR2017BC042), the Forestry Science and Technology Innovation Project of Shandong Province (Grant No. LYCX10-2018-50), the Key Special Foundation for the National Key Research and Development Program of China (Grant No. 2016YFD0600704) and the National Natural Science Foundation of China (Grant Nos. 31700497, 31300479).

Author contributions

JW, ZY, XD and YL designed the experiment. JW, ZY, YS, CW and JF performed the whole experiments. JW and YS drew the figures. GK and RZ carried out the evaluation of magnetic properties of the aerogels. JW, XD and YL wrote the paper. Everybody comments on the final manuscript.

Compliance with ethical standards

Conflict of interest The authors declare that they have no conflict of interest.

Electronic supplementary material: The online version of this article (https://doi.org/10.1007/s10853-019-03322-0) contains supplementary material, which is available to authorized users.

References

[1] Wang Q, Yang ZM (2016) Industrial water pollution, water environment treatment, and health risks in China. Environ Pollut 218:358–365

[2] Li QY, Zhou DD, Zhang PL, Man P, Tian ZB, Li Y, Ai SY (2016) The BiOBr/regenerated cellulose composite film as a green catalyst for light degradation of phenol. Colloid Surface Physicochem Eng Aspect 501:132–137

[3] Wang JL, Chen C (2009) Biosorbents for heavy metals removal and their future. Biotechnol Adv 27(2):195–226

[4] Bao LJ, Maruya KA, Snyder SA, Zeng EY (2012) China's water pollution by persistent organic pollutants. Environ Pollut 163:100–108

[5] Sun JC, Fan H, Nan B, Ai SY (2014) Fe_3O_4@LDH@Ag/Ag_3PO_4 submicrosphere as a magnetically separable visible-light photocatalyst. Sep Purif Technol 130:84–90

[6] Jiang WJ, Wu LN, Duan JL, Yin HS, Ai SY (2018) Ultrasensitive electrochemiluminescence immunosensor for 5-hydroxymethylcytosine detection based on Fe_3O_4@SiO_2 nanoparticles and PAMAM dendrimers. Biosens Bioelectron 99:660–666

[7] Shen LL, Zhang GR, Li W, Biesalski M, Etzold BJM (2017) Modifier-free microfluidic electrochemical sensor for heavy-metal detection. ACS Omega 2(8):4593–4603

[8] Cao CY, Cui ZM, Chen CQ, Song WG, Cai W (2010) Ceria hollow nanospheres produced by a template-free microwave-assisted hydrothermal method for heavy metal ion removal and catalysis. J Phys Chem C 114(21):9865–9870

[9] Phoebe ZR, Heather JS (2015) Inorganic nano-adsorbents for the removal of heavy metals and arsenic: a review. RSC Adv 5:29885–29907

[10] Wang XQ, Liu WX, Tian J, Zhao ZH, Hao P, Kang XL, Sang YH, Liu H (2014) Cr(VI), Pb(II), Cd(II) adsorption properties of nanostructured BiOBr microspheres and their application in a continuous filtering removal device for heavy metal ions. J Mater Chem A 2:2599–2608

[11] Mercy RB, Siddulu NT, Stalin J, Kavitha R, Gurwinder S, Jessica S, Ugo R, Khalid AB, Ajayan V (2018) Recent advances in functionalized micro and mesoporous carbon materials: synthesis and applications. Chem Soc Rev 47:2680–2721

[12] Chen CJ, Song JW, Zhu SZ, Li YJ, Kuang YD, Wan JY, Kirsch D, Xu LS, Wang YB, Gao TT, Wang YL, Huang H, Gan WT, Gong A, Li T, Xie J, Hu LB (2018) Scalable and sustainable approach toward highly compressible, anisotropic, lamellar carbon sponge. Chem 4(3):544–554

[13] Yin K, Yang S, Dong XR, Chu DK, Duan JA, He J (2018) Robust laser-structured asymmetrical PTFE mesh for underwater directional transportation and continuous collection of gas bubbles. Appl Phys Lett 112(24):243701. https://doi.org/10.1063/1.5039789

[14] Yin K, Chu DK, Dong XR, Wang C, Duan JA, He J (2017) Femtosecond laser induced robust periodic nanoripples structured mesh for highly efficient oil–water separation. Nanoscale 9:14229–14235

[15] Kabiri S, Tran DNH, Azari S, Losic D (2015) Graphene-diatom silica aerogels for efficient removal of mercury ions from water. ACS Appl Mater Interfaces 7(22):11815–11823

[16] Fu JJ, He CX, Wang SQ, Chen YS (2018) A thermally stable and hydrophobic composite aerogel made from cellulose nanofibril aerogel impregnated with silica particles. J Mater Sci 53(9):7072–7082. https://doi.org/10.1007/s10853-018-2034-9

[17] Jiang F, Liu H, Li YJ, Kuang YD, Xu X, Chen CJ, Huang H, Jia C, Zhao XP, Hitz E, Zhou YB, Yang RG, Cui LF, Hu LB (2018) Lightweight, mesoporous, and highly absorptive all-nanofiber aerogel for efficient solar steam generation. ACS Appl Mater Interfaces 10(1):1104–1112

[18] Chavan AA, Li HB, Scarpellini A, Marras Sergio, Manna L, Athanassiou A, Fragouli D (2015) Elastomeric nanocomposite foams for the removal of heavy metal ions from water. ACS Appl Mater Interfaces 7(27):14778–14784

[19] Gu XY, Yang Y, Hu Y, Hu M, Wang CY (2015) Fabrication of graphene-based xerogels for removal of heavy metal ions and capacitive deionization. ACS Sustain Chem Eng 3(6):1056–1065

[20] Lamymendes A, Rui FS, Durães L (2018) Advances in carbon nanostructure-silica aerogel composites: a review. J Mater Chem A 6:1340–1369

[21] Zhu HL, Luo W, Ciesielski PN, Fang ZQ, Zhu JY, Henriksson G, Himmel ME, Hu LB (2016) Wood-derived materials for green electronics, biological devices, and energy applications. Chem Rev 116(16):9305–9374

[22] Santos SM, Carbajo JM, Gómez N, Ladero M, Villar JC (2017) Paper reinforcing by in situ growth of bacterial cellulose. J Mater Sci 52(10):5882–5893. https://doi.org/10.1007/s10853-017-0824-0

[23] Tian Zhengbin, Zong Lei, Niu Rujie, Wang Xiao, Li Yan, Ai Shiyun (2015) Recovery and characterization of lignin from alkaline straw pulping black liquor: as feedstock for bio-oil research. J Appl Polym Sci 132:42057–42065

[24] Yue YY, Han JQ, Han GP, Aita GM, Wu QL (2015) Cellulose fibers isolated from energycane bagasse using alkaline

and sodium chlorite treatments: structural, chemical and thermal properties. Ind Crops Prod 76:355–363

[25] Nair SS, Kuo PY, Chen HY, Yan N (2017) Investigating the effect of lignin on the mechanical, thermal, and barrier properties of cellulose nanofibril reinforced epoxy composite. Ind Crops Prod 100:208–217

[26] Zhuo X, Liu C, Pan RT, Dong XY, Li YF (2017) Nanocellulose mechanically isolated from *Amorpha fruticosa* Linn. ACS Sustain Chem Eng 5(5):4414–4420

[27] Zhuo X, Wei J, Xu JF, Pan RT, Zhang G, Guo YL, Dong XY, Long L, Li YF (2017) Nanocellulose isolation from *Amorpha fruticosa* by an enzyme-assisted pretreatment. Appl Environ Biotech 2:34–39

[28] Huang JD, Wang SQ, Lyu SY, Fu F (2018) Preparation of a robust cellulose nanocrystal superhydrophobic coating for self-cleaning and oil–water separation only by spraying. Ind Crops Prod 122:438–447

[29] Zhang XT, Jing SS, Chen ZH, Zhong LX, Liu QZ, Peng XW, Sun RC (2017) Fabricating 3D hierarchical porous TiO_2 and SiO_2 with high specific surface area by using nanofibril-interconnected cellulose aerogel as a new biotemplate. Ind Crops Prod 109:790–802

[30] Chen CJ, Hu LB (2018) Nanocellulose toward advanced energy storage devices: structure and electrochemistry. Acc Chem Res. https://doi.org/10.1021/acs.accounts.8b00391

[31] Osorio DA, Seifried B, Moquin P, Grandfield K, Cranston ED (2018) Morphology of cross-linked cellulose nanocrystal aerogels: cryo-templating versus pressurized gas expansion processing. J Mater Sci 53(13):9842–9860. https://doi.org/10.1007/s10853-018-2235-2

[32] Zhu H, Yang X, Cranston ED, Zhu SP (2016) Flexible and porous nanocellulose aerogels with high loadings of metal–organic-framework particles for separations applications. Adv Mater 28(35):7652–7657

[33] Geng BY, Wang Y, Wu S, Ru J, Tong CC, Chen YF, Liu HZ, Wu SC, Liu XY (2017) Surface-tailored nanocellulose aerogels with thiol-functional moieties for highly efficient and selective removal of Hg(II) ions from water. ACS Sustain Chem Eng 5(12):11715–11726

[34] Yao C, Wang F, Cai Z, Wang X (2016) Aldehyde-functionalized porous nanocellulose for effective removal of heavy metal ions from aqueous solutions. RSC Adv 6:92648–92654

[35] Liu HZ, Geng BY, Chen YF, Wang HY (2017) Review on the aerogel-type oil sorbents derived from nanocellulose. ACS Sustain Chem Eng 5(1):49–66

[36] Shaghaleh H, Xu X, Wang S (2018) Current progress in production of biopolymeric materials based on cellulose, cellulose nanofibers, and cellulose derivatives. RSC Adv 8:825–842

[37] Song JW, Chen CJ, Yang Z, Kuang YD, Li T, Li YJ, Huang H, Kierzewski I, Liu BY, He SM, Gao TT, Yuruker SU, Gong A, Yang B, Hu LB (2018) Highly compressible, anisotropic aerogel with aligned cellulose nanofibers. ACS Nano 12:140–147

[38] An F, Li XF, Min P, Li HF, Dai Z, Yu ZZ (2018) Highly anisotropic graphene/boron nitride hybrid aerogels with long-range ordered architecture and moderate density for highly thermally conductive composites. Carbon 126:119–127

[39] Zhu Y, Zheng Y, Wang F, Wang A (2016) Fabrication of magnetic macroporous chitosan-g-poly (acrylic acid) hydrogel for removal of Cd(2+) and Pb(2.). Int J Biol Macromol 93(Part A):483–492

[40] Fu F, Chen R, Xiong Y (2006) Application of a novel strategy—coordination polymerization precipitation to the treatment of Cu^{2+}-containing wastewaters. Sep Purif Technol 52(2):388–393

[41] Lu N, Bu YX, Luo GM (2017) Cu-wire-mediated dipyrimidine base pairs as the building blocks for conductive and magnetic Cu–DNA nanowires. J Math Chem 55(6):1301–1321

[42] Shang K, Sun B, Sun JC, Li J, Ai SY (2013) Poly-(3-thiopheneacetic acid) coated Fe_3O_4@LDHs magnetic nanospheres as a photocatalyst for the efficient photocatalytic disinfection of pathogenic bacteria under solar light irradiation. New J Chem 37:2509–2514

[43] Gao H, Liu Y, Zeng G, Xu W, Li Y, Xia W (2008) Characterization of Cr(VI) removal from aqueous solutions by a surplus agricultural waste–rice straw. J Hazard Mater 150(2):446–452

[44] Aliabadi M, Morshedzadeh K, Soheyli H (2006) Removal of hexavalent chromium from aqueous solution by lignocellulosic solid wastes. Int J Environ Sci Technol 3(3):321–325

[45] Dehghani MH, Taher MM, Bajpai AK, Heibati B, Tyagi I, Asif M, Agarwal S, Gupta VK (2015) Removal of noxious Cr(VI) ions using single-walled carbon nanotubes and multi-walled carbon nanotubes. Chem Eng J 279:344–352

[46] Dubey SP, Gopal K (2007) Adsorption of chromium(VI) on low cost adsorbents derived from agricultural waste material: a comparative study. J Hazard Mater 145(3):465–470

[47] Garg UK, Kaur MP, Garg VK, Sud D (2007) Removal of hexavalent chromium from aqueous solution by agricultural waste biomass. J Hazard Mater 140:60–68

[48] Babel S, Kurniawan TA (2004) Cr(VI) removal from synthetic wastewater using coconut shell charcoal and commercial activated carbon modified with oxidizing agents and/or chitosan. Chemosphere 54(7):951–967